ORIGINAL ARTICLE

J. Mazumder · A. Schifferer · J. Choi

Direct materials deposition: designed macro and microstructure

Abstract Solid freeform fabrication of engineering materials is now possible using the Direct Metal Deposition (DMD) technique. Closed loop optical feedback system for DMD makes realistic components with dimensional accuracy of 0.01 inch. On the other hand, close control of the process parameter can provide microstructure of choice. Such continued capability to control macro and microstructure is creating considerable interest. H13 tool steel is one of the difficult alloys for deposition due to residual stress accumulation from martensitic transformation. However, it is the material of choice for the die and tool industry. DMD offers Copper chill blocks and water cooling channels as the integral part of the tool. On the other hand ZrO_2 was co-deposited with nickel superalloys using DMD. This process thus is amenable to produce both macro and microstructure to a designed specification. This paper briefly reviews the state of the art of DMD and describes the microstructure and mechanical properties of selected engineering alloy systems deposited by DMD.

Key words Direct metal deposition · Solid free form fabrication · Laser cladding · H13 tool steel · Microstructure · Optical feedback · Dendrite arm spacing · Rapid fabrication of die and mold · Surface roughness · Ceramic-metal co-deposition

Introduction

One of the most recognized problems in the U.S. is the time it takes to get technology and hence products to the market. In manufacturing the limiting time for many products is the design and fabrication of molds and dies

J. Mazumder (✉) · A. Schifferer · J. Choi
Center for Laser Aided Intelligent Manufacturing,
University of Michigan, 2250 G. G. Brown, 2350 Hayward,
Ann Arbor, MI 48109-2125, USA
e-mail: mazumder@engin.umich.edu
Fax: +1- 647 3170

Present address:
J. Mazumder, Caterpillar Company, Illinois

of all types. It is not unusual for large complicated dies to take from weeks to months to almost a year before they are ready to manufacture product. Stereolithography has been a help in design process to visualize a component produced directly from CAD data base by curing polymers with lasers. Most manufacturers are looking for a device that can make a product directly from a CAD drawing with a designed macro and microstructure. Repair procedures are also needed for metals that do not change the material properties and result in reduced life for the product.

The preliminary work on Direct Metal Deposition of Aluminum has been demonstrated to provide metal properties equivalent to a wrought process thus making it potentially useful for the direct fabrication of parts and dies [1]. Almost all other known processes that are developing metal result in a sintered product due to trapping of oxides and the inability to totally bond. As a result they need to try to fill the metal matrix and do not provide the strong properties demonstrated by DMD. If there is a total bonding and no oxides or sintered properties the metal property has generally been significantly affected as is the case in a welded type structure which is built up by repeated passes. In these cases significant heat treatment is needed to make the part useful and relieve the stresses. Laser aided DMD limits these problems since it creates a very small heat affected zone. DMD can be used on almost any surface and can mix metals to create a variety of properties including graded structure. Only other process exhibiting similar potential is droplet based manufacturing [2, 3, 4, 5, 6]. However, DMD has wider range of deposition capability.

The DMD process should have no effect on environmental concerns since the process is an additive one and not one that creates waste products. It is carried out in an inert atmosphere with powdered metal being dropped on the point and melted at that spot. Health and safety concerns only appear to be the result of laser operations and there are procedures for these conditions available.

A recent survey made by National Center for Manufacturing Science (NCMS) revealed that DMD can re-

Table 1 Direct metal freeform fabrication processes

Process	Deposition Type	Accuracy: Horizontal	Layer Thickness	Deposition Rate	Materials	References
SLS	Laser Sintering	High	N/A	N/A	steel, Co brazing	8–9
SDM	Droplet based, & Cladding	N/A Machined finish	Variable	30 g/min	Stainless Steel, INVAR™	10–11
Welding	Welding	0.2 to 0.5 mm	up to 50 mm	N/A High	Steels; Numerous	12–14
Droplet Based FF	Droplet Based	N/A	N/A	25 to 150 micron dia. droplets	Bi-Sn	2–6,15
LENS	Cladding	0.02 mm Z: 0.4 mm	0.13 to 0.38 mm	N/A Low	SS,Alloys, Numerous	16–18
DLF	Cladding	0.075 to 0.125 mm	0.075 to 0.125 mm	1 to 2 g/min	SS, P20, Numerous	19, 20
DMD at Michigan	Cladding	N/A	0.254 mm	0.1 to 4.1 cm³/min	H13, Al, Numerous	1, 21, 22

duce the time for die production by 40% [7]. The DMD process allows for either the direct production of a part or short time low cost delivery of molds or dies. When perfected the process will greatly reduce their costs and time to getting a prototype or product ready for use. This is an example of a situation that would benefit a wide variety of products for both defense and commercial sectors. The ability to make low volume high quality parts directly from CAD is applicable to most of the DOD manufacturers. The Navy has also expressed interest in this process as it would allow an aircraft carrier to go out with barrels of metal and CAD drawings to make parts as they are needed and not carry a large inventory of spare parts. The automotive and electronics industry sees the application for rapid fabrication of dies. Direct metal freeform fabrication has the ability to create full functional parts from metal powder. Table 1 summarizes the current technologies in direct metal part fabrication.

The potential for the DMD process is currently limitless. Many groups are actively pursuing it for commercial possibilities. The direct fabrication of molds and dies and the repair of these parts is the most obvious application. However, fabrication of low volume parts has not been fully analyzed and may be the biggest potential for this process. Surgical instruments have been explored and the potential savings are in the hundreds of millions of dollars. For surgical tools, DMD can reduce 62 steps into 7 steps [7]. The use of the process in the aerospace business is another huge area for applications.

The scientific challenge is to control the dimension and properties. Close control of dimension will result in substantial savings in post process machining cost for surface finish. Substantial cost reduction is possible, if desired properties can be achieved through process control and minimize post process heat treatment. Control of the melt pool size and solidification time can offer both desired dimension by limiting the melt pool volume and desired properties through microstructure manipulation by controlling the cooling rate. This will require quantitative understanding of the relationship between inde-

pendent process parameters (Laser power speed, powder deposition rate etc.), dimension, cooling rate. microstructure and properties by developing fundamental understanding of the associated transport phenomena. Strategies for on-line process control will also be required to achieve the desired melt pool volume and cooling rate.

Experimental

In this DMD technique laser generates a melt pool on a substrate material while a second material is delivered into the melt pool either as powder or as wirefeed which melts and forms metallurgical bond with the substrate (see Fig. 1). Turbine disc of circular geometry was produced by Brienan and Kear [23] via layer by layer laser cladding around 1978. Present computer controlled 5-axis workstations integrated with lasers enable us to fabricate various geometry. Either CO_2 or Nd-YAG lasers can be used as the laser source. The system at University of Michigan includes a 6 kw RF excited CO_2 Laser integrated with a 5-axes work station controlled by a Allan Bradley 8400 controller. The laser has the capability to
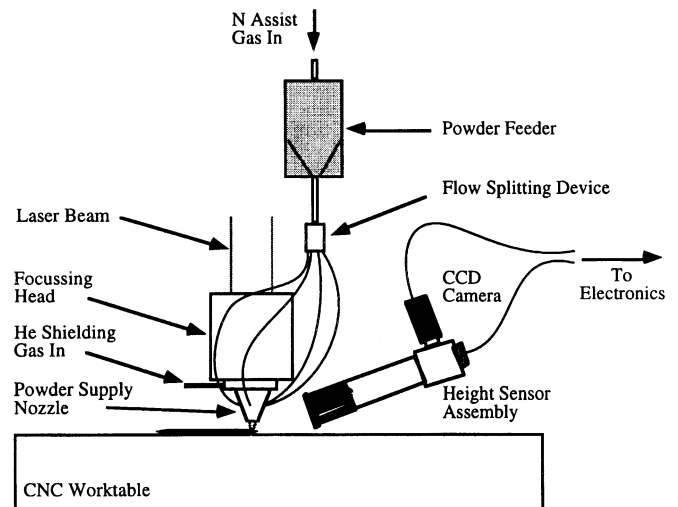
Fig. 1
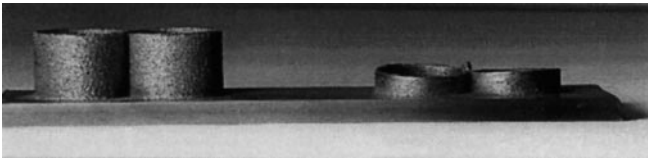
Fig. 2 Example of fabrication with height controller. Left: w/height controller, Right: no height controller

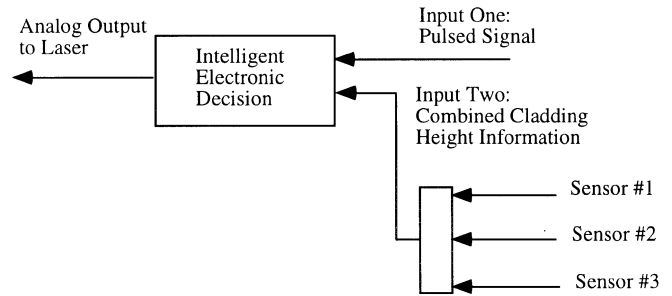**Fig. 4** Height controller with multiple sensor inputs
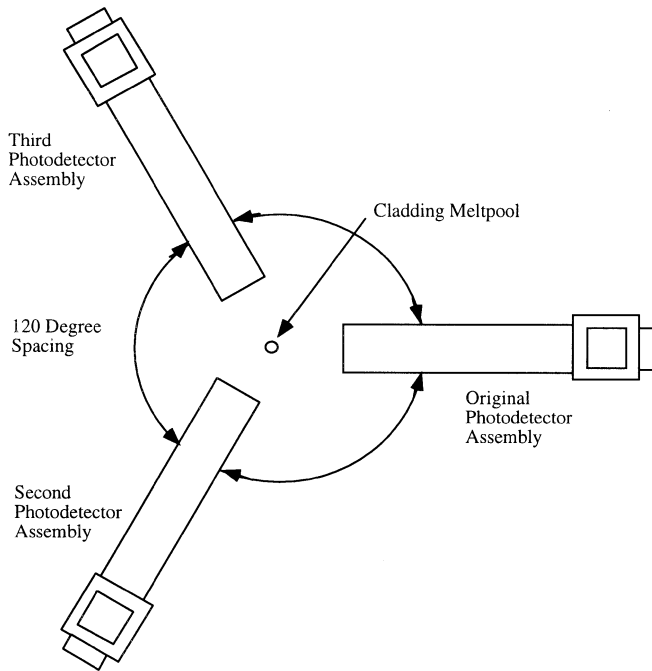
Fig. 3 Multiple sensor layout. Top view

operate between 0–6 kw and the work station has a traverse speed range of 0–400 ipm (0–169.3 mm/sec). It has a work envelop of 1 m×0.5 m×0.5 m and carry up to half a ton.

Powder can be delivered either from the side with an independent nozzle or with a concentric nozzle where beam and powder come through the same nozzle. The concentric nozzle designed based on a patent [24] (U.S.Patent # 4724255) and offers equal deposition rates in any direction. Inert gas flown through the nozzle helps both in powder delivery and shielding the deposit from oxidation. Shielding strategy is a delicate balance between powder delivery without causing excessive disturbance at the melt pool, but adequate to drive away the ambient air. Side injection nozzle can build up volume rapidly whereas, the concentric nozzle can provide better resolution. In an ideal system rotating head with both nozzles should be available.

Control of the deposit thickness or height is a critical issue since it impacts on the quality of the product. Visualization and measurement of the surface deformation of the melt pool is possible by Reflective Topography technique developed at the University of Illinois [25]. In order to control the deposit dimension, a feed-back loop to control the process parameters was designed and executed [26]. Another technique for on-line monitoring of height and composition of the deposit is also developed but presently working in open loop only [27].

The basic function of the height controller is to limit the maximum height of metal deposition. Following is a simple example of the controller function. Shown in Fig. 2 are two samples produced by laser cladding, each of which have a deposition path of two overlapping circles. After multiple cladding layers are placed one

at a time on top of the previous layers, a pair of overlapping cylinders is fabricated. The sample on the right is produced without any height control and it can be seen that there is excess cladding build-up where the circles overlapped. The overall height at this location is approximately twice that of the cylinders height because the laser cladding passes this point twice per layer, laying down the same amount of material during each pass. In the other areas besides the overlap, it can be seen that the overall height is uneven. The sample on the left in Fig. 2 was fabricated using the height controller. The height controller has the ability to sense the cladding layer is building up higher in the overlapping region, and it shuts off the laser until it is past the area of excess build-up. In this case, the layer thickness was set at 0.1778 mm, and 100 layers were subsequently built up from the substrate. As a result, the overall height was held to 17.78 mm with a variation of less than 0.075 mm. For this reason, the height controller is a necessity in order to fabricate accurate macroscopic shapes.

One can either use one sensor or multiple sensors for close-loop feed-back control of the deposit height. Multiple sensors will overcome any problem related to the field of view with respect to the cladding direction for a single sensor. Figure 3 shows a top view of the ideal layout of the three sensors, which are equally spaced 120 degrees apart. For the actual layout of the sensors for this study, the second sensor was only 90 degrees from the first sensor. This uneven spacing did not cause any problems since the sensors are effective up to 180 degrees. Since two more sensors were added to the system, the signal processor also had to be modified. In order to input one signal into the processor, the three sensor signals were combined through several logic gates before they were sent to the processor. The new flow diagram for the height controller is shown in Fig. 4.

Process parameter matrix

There are two major areas of the direct metal deposition processing that were investigated. The first area that was studied was the laser processing parameters and how they affected the multiple characteristics of the fabricated samples. The other area that was studied was the effect of multiple height control sensors on the characteristics of the final parts. Also, effects of some controller parameters on material processing were investigated. A statistically designed experimental matrix was used for this study. Below is a table that summarizes the independent process parameters that were considered (Table 2).

In all of the experiments that were carried out, the melt pool diameter was used at a size of 0.7 mm or slightly larger from defocusing. The powder flow assist gas and the shielding gas to be used in all cases are Nitrogen and Helium, respectively. These are gases that have been shown to be effective for this process from previous research of direct metal deposition in the CLAIM laboratory of University of Michigan. The height controller was used in the building of specimens in order to prevent any uneven build-up of specimens. This controller altered the effective power of the laser for all samples, so the duty cycle needs to be taken into account during specimen analysis. The duty cycle was typically held at 70%, with a variation of 20%, depending on how well the inde-

Table 2 Independent processing parameters

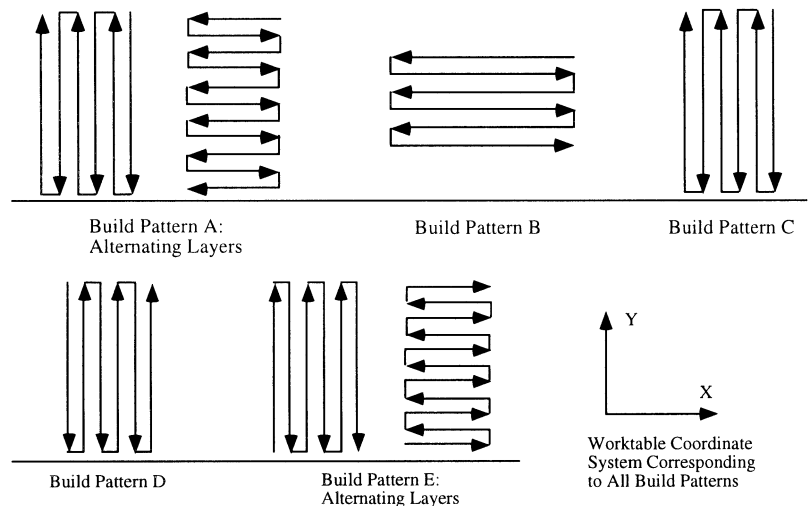| Independent Parameter	Low	Medium	High
Laser Power (watts)	700	950	1200
Powder Flow (grams/min)	4.0	6.0	8.0
Traverse Speed (mm/s)	8.5	17	25.4
Assist Gas (liters/min)	2.36 (5 SCFH)	4.72 (10 SCFH)	7.08 (15 SCFH)
Shielding Gas (liters/min)	4.72 (10 SCFH)	7.08 (15 SCFH)	9.44 (20 SCFH)
Pass Overlap (% width)	14.5, 23	31.5, 40, 48.5	57, 67
Number of Sensors	1	–	3
Controller Reset Time (ms)	5, 10	20, 33	66, 100
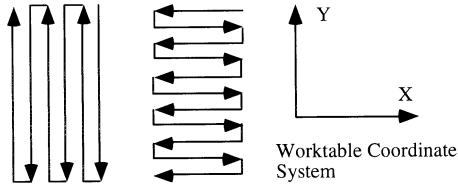
Fig. 5 Build pattern of samples

pendent parameters were matched with the specified layer thickness. This duty cycle is essentially the average time that the laser is on with respect to total processing time. The percent clad width overlap remained at the previously used value of 27%, except during the testing of percent pass overlap. The component that was built in each experiment was approximately 7.6 mm wide, 15.25 mm long, and 5.1 mm tall. The build pattern used for these specimens is shown in Fig. 5.

Effect of multiple sensors

In order to identify any improvements due to adding multiple sensors to the height controller, several build patterns were tested for each a single sensor and multiple sensor height controller. The build patterns used are shown in Fig. 6. These build patterns were chosen because they are the basics of all of build conditions that the direct metal deposition process may be exposed to. Any other cladding pattern, such as a circle or a triangle, is a combination of these primary build patterns.

The parameters used for this testing were found to produce good cladding from the fabrication above, and are as follows: 700 watts laser power, 5.6 grams/minute powder flow rate, 17 mm/s traverse speed, and 27 percent pass width overlap. These parameters were held constant throughout this testing, except for one set

of tests in which the percent overlap was increased to 74 percent. In this last case, both A and E build patterns were used.

Specimen analysis

The following types of analysis were used in comparing the specimens resulting from the different studies:

• Microhardness testing for selected samples
• Microstructure and porosity evaluation for all samples
• Surface roughness for selected samples
• Deposit thickness for selected samples
• Percent powder utilization for selected samples

The equipment that was used in the analysis of the fabricated samples is described below.

Mechanical testing

All microhardness testing was completed using a Buehler Vickers microhardness test machine. In order to find the best test parameters, several different loads and load times were tested and hardness variation was found to be minimal. Also, similar etched and non-etched areas were tested and there was no variation in the microhardness results. All testing was done on polished and etched surfaces using a 300 gram load for 10 seconds.

Macrohardness testing was carried out on a Wilson Hardness test machine. A Roc kwell C indenter was used along with the required 150 kg load. The calibration of the machine was verified using a certified calibration block.

Microstructure and density analysis

All samples were etched 30 to 60 seconds using a four percent solution of Nitric acid. Microstructure images were captured using a

Fig. 6 Build patterns used to test height controller capabilities

Build Pattern A: Alternating Layers

Build Pattern B

Build Pattern C

Build Pattern D

Build Pattern E: Alternating Layers

Worktable Coordinate System Corresponding to All Build Patterns

Table 3 H13 composition by weight percent

C	Si	Mn	Cr	Mo	V	P	S	O	N	Fe
0.40	0.93	0.35	5.31	0.30	1.07	0.016	0.005	0.006	0.048	balance

Nikon optical microscope and Scion Image version 1.59 software. This same software was used to analyze a cross-sectional image of the polished specimen to determine the amount of porosity. This percent of porosity is assumed to be similar to that of the overall specimen, therefore estimating the percent full theoretical density.

Roughness measurement

To measure the surface roughness, the following equipment was used: a Taylor Hobson Form Talysurf inductive profilometer with a 2.5 micron radius diamond stylus. Two types of roughness measurements were used in the surface analysis; profile roughness average (PRa) and maximum profile roughness height (PRt). The maximum profile roughness height (PRt) is the distance between the lowest and highest points on a surface.

Powder properties

The AISI H13 tool steel powder used in the fabrication of samples was induction melted and nitrogen atomized. The powder was –70 mesh size and had the following composition:

This powder was produced at Crucible Research, a division of Crucible Materials Corporation.

Results and discussion

Layer thickness

There is a large range of layer thicknesses as well as deposition rates for laser cladding, but the range seen here is on the smaller end due to the fact that this is "fine" cladding. Some of the thicker layers and deposition rates in this study approached those of typical cladding. Both the layer thickness and the volume deposition rates were affected predominately by the specific energy and powder mass flow rate. Specific energy is defined as follows:

$$S.E. = \frac{Laser\ Power}{Meam\ Diameter \times Velocity}$$

Note: For comparison purposes, the adjusted specific energy will be used instead of just specific energy because the height control system was used during the processing of the samples. This height feed-back controller controlled the duty cycle of the laser beam, making the actual power the same or less than the original set laser power. The adjusted specific energy is calculated the same as specific energy, but the average power output is used as opposed to the full power output. For example, if the base laser power is set at 1000 watts, but the laser is turned on only 70% of the time (70% duty cycle) then the average power would be taken as 700 watts. As shown in Fig. 7 there is a positive linear relationship between the layer thickness and specific energy for each powder mass flow rate. The resulting layer thicknesses ranged from 0.08 mm per layer to 1.37 mm per layer. In the percent width overlap study, the layer thicknesses ranged from 0.15 mm to 0.37 mm for 13% to 67% pass width overlap, respectively. The layer thickness increased more initially, as percent overlap in-
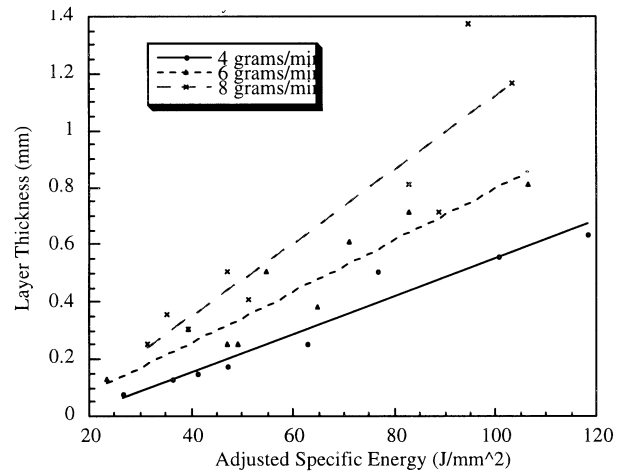
Fig. 7 Influence of adjusted specific energy and powder flow rate on layer thickness
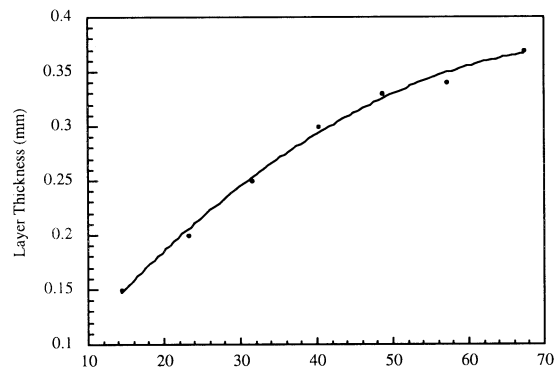
Fig. 8 Influence of% pass width overlap on layer thickness
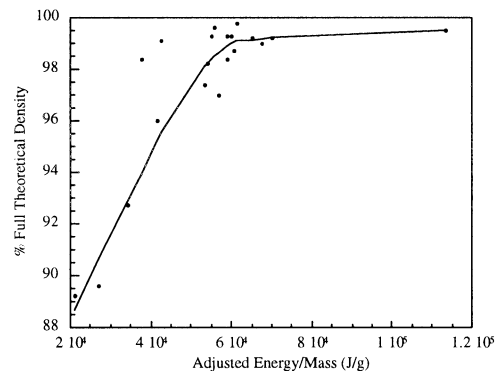
Fig. 9 Influence of adjusted energy/mass on material density

creases from 10 to 20 percent. When the percent overlap passed 40%, the amount of layer increase per percent overlap increase started to level off. This is shown in Fig. 8.

Figure 9 shows a plot of energy per unit mass deposited and the associated densities. It can be clearly seen that
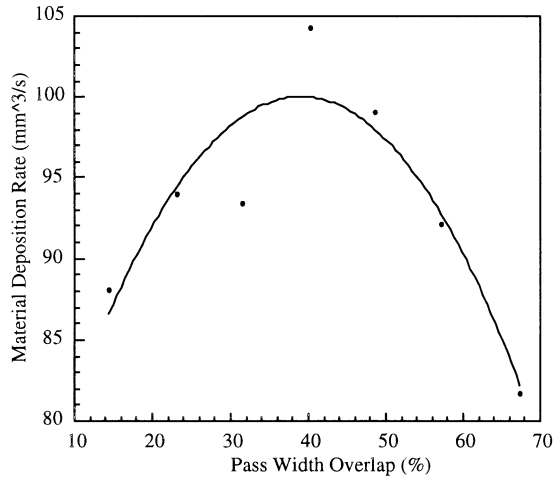
Fig. 10 Effect of percent pass overlap on material deposition rate

when the energy per unit mass deposited drops below 40 kilojoules per gram, the density drops below 96 percent full theoretical density. Another reason for the porosity is that as the layers get thicker, the power density of the laser beam gets lower toward the bottom of the clad bead due to the laser beam becoming more defocused. In order to show this, the melt pool diameter was measured at several different distances from the point of laser focus. This was accomplished by burning a steel plate with the laser beam at the different distances from focus so that the melt pool diameters could be measured. If the power density at the typical processing region (0.76 mm from focus) is taken as 100%, then the power density towards the bottom of the cladding for the thicker layers (1.5 to 2.2 mm from focus) the power density drops to approximately 90%. Because of this lower power density the laser can not fully melt the powder that is deposited at that level, and it does not have enough power to melt into the substrate material, which is necessary to cause a good bond. This would also cause the energy per mass ratio to be lower, as observed above.

To prevent porosity, the layer thickness should be less than 0.7 mm, and the energy per mass caught ratio should be measured to ensure that porosity is not occurring. Another solution is to reduce the powder flow rate, therefore reducing the amount of potential powder to be caught by the melt pool. The percent overlap has a significant effect on the deposition rate. Figure 10 shows that around 40% overlap, the volume deposition rate reaches its maximum value of approximately 104 mm³/s. Above and below 40 percent overlap, the volume deposition rate gets smaller due to the percent overlap and layer thickness reaching their best combination at 40 percent overlap. This is a very important factor, because optimizing the percent overlap can possibly reduce processing time up to 10–15 percent. Another parameter that should be optimized is powder efficiency.
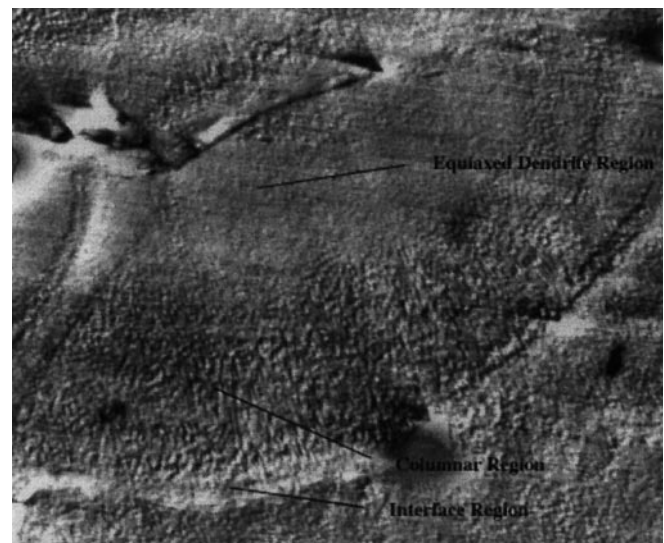
Influence of gas flow rates

The assist and shielding gas flow rates did have a significant effect on the clad quality when they were turned down around 2.36 and 4.72 liters/min (5 to 10 SCFH), respectively. Once the gas flow rates were in this range, excess powder from previous cladding passes was not blown out of the way of the laser, and therefore the laser would just melt the surface of the excess powder, making a shell-like structure. This resulted in the clad being mostly loose powder and prevented normal cladding from taking place.

To prevent any unusual cladding build-up as previously mentioned, the absolute minimum gas flow rates that should be used are 4.72 and 7.08 liters/min. (10 and 15 SCFH) for the assist and shielding gases, respectively. It is also important for the assist gas flow rate to be lower than the shielding gas flow rate. A higher shielding gas flow rate seemed to help to remove excess powder from the surface where deposition was taking place. Keeping this flow rate higher will prevent any back flow of particles into the nozzle, which is important for keeping the laser optics and the powder delivery nozzle clean.
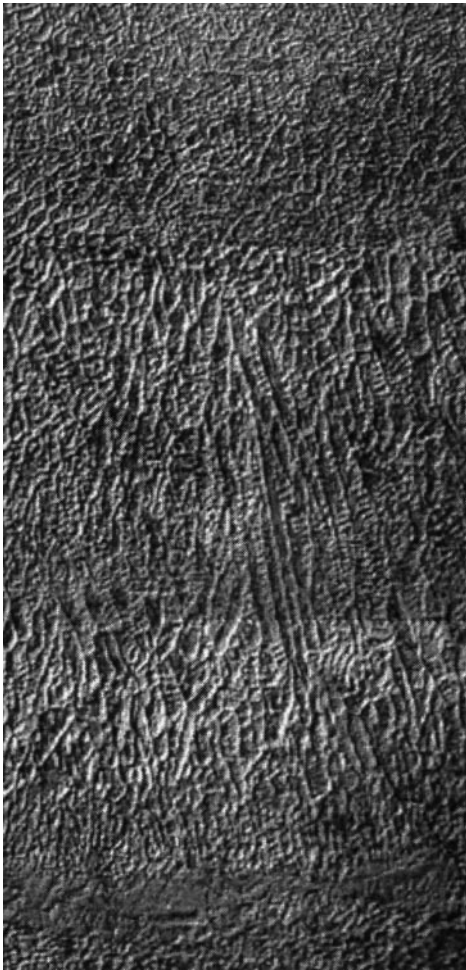
The direct metal deposition process has a unique effect on the physical properties of the metal being processed. This ranged from microstructure variation within the same material as well as mechanical properties' variation. Hardness, roughness, porosity, as well as strength and ductility were affected by changing parameters.

Microstructure analysis

The microstructure over the range of parameters used ranged from columnar grains to equiaxed grains, most of these grains containing martensite. The primary and sec-
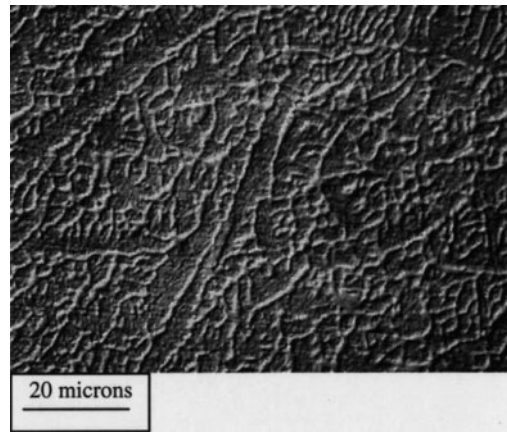

Fig. 11 Cladding cross-section

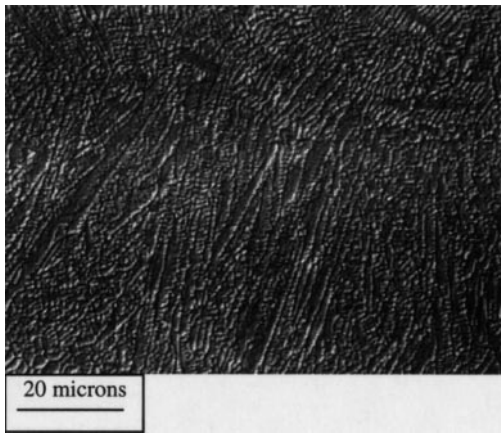**Fig. 12** Close-up of interface, columnar and equiaxed dendrite regions

Fig. 13 Large dendrite microstructure; power =1200 W, velocity = 8.5 mm/s, powder = 8.0 grams/min, layer thickness = 1.37 mm, pass overlap = 27%

directions at once, each growth direction representing a similar temperature gradient. This is called the equiaxed region and is shown towards the top of Fig. 12. It was also found that this microstructure stays consistent throughout a single sample.

Effects of process parameters

There is a definite change in microstructure as the direct metal deposition processing parameters are changed. Two extreme cases of the range of microstructure that were observed are shown in Figs. 13 and 14. The first specimen had a power of 1200 watts, a traverse speed of 8.5 mm/s, a powder flow rate of 8.0 grams/min, a layer thickness of 1.37 mm, and a 27% pass width overlap. In the first case, the grains are large and mostly equiaxed, approximately 10 to 16 microns across. These large dendrites are due to a high specific energy as well as a high material deposition rate of 290 mm³/s. With a high specific energy as well as a larger amount of molten material being added, the solidifying material is held at a higher temperature for a longer amount of time and therefore the local temperature gradients are smaller. This allows the grains to time grow, and in no specific direction. On the other hand, the microstructure shown in Fig. 14, is much finer, having a small interface region and a predominant columnar region. This specimen had a processing power of 1200 watts, a traverse speed of 50.8 mm/s, a powder mass flow of 4.8 grams/min, a layer thickness of 0.254 mm, and a pass width overlap of 66%. The fine microstructure in this specimen is due to a lower specific energy as well as a smaller material addition rate. The speed of the cladding in this case is six times faster that of the previous case, therefore there is not time for the laser to have any type of annealing effect on the material. The amount of molten metal is thinner and therefore the local temperature gradient is going to be higher throughout the whole cladding pass. This is why

ondary dendrite arms spacing, and hence cooling rate, were also affected by the changing parameters.

Inherent to the process, a part made by the direct metal deposition process is composed of multiple cladding passes. A picture of a central single cladding pass is shown in Fig. 11. The parameters for this specimen are as follows: 700 watts laser power, 6.0 grams/min powder flow, 17 mm/sec and 0.254 mm layer thickness. As is pointed out in Fig. 11, each cladding pass is composed of typically three different regions. These are the interface, the columnar grain, and the equiaxed grain regions. The interface region, Fig. 11, is where the laser remelts and/or reheats the substrate material and begins to add the new cladding material. This will result in heat treating the existing grains, allowing the grains time to grow slightly larger. Above the interface, the grains are more columnar, as a result of directional cooling, and are aligned with the largest temperature gradient during cooling. Because the heat is flowing out of the clad towards the substrate material, the grains, or primary dendrites, are very long, slender and perpendicular to the interface. When the temperature gradient is similar in several directions, the grains can grow in several different
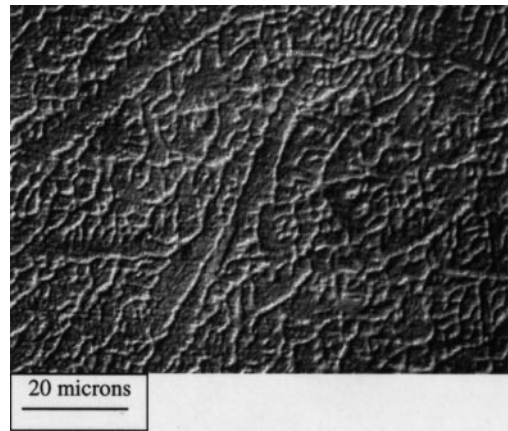
Fig. 14 Fine dendrite microstructure; power =1200 W, velocity = 50.8 mm/s, powder = 4.8 grams/min, layer thickness = 0.254 mm, pass width overlap = 66%
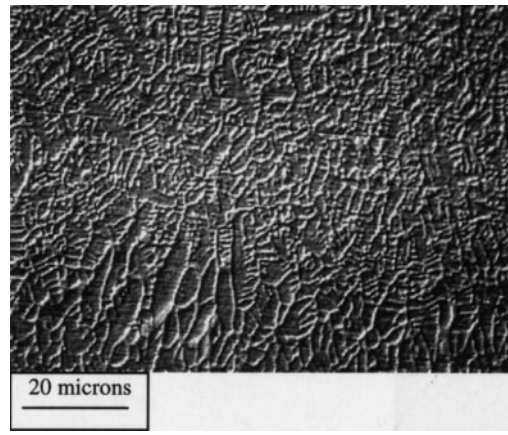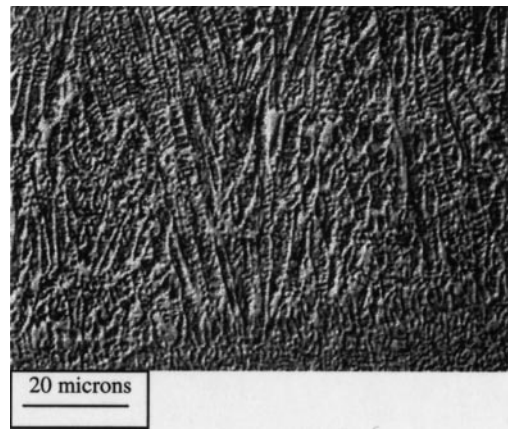

Fig. 15 Sample C16. 200 J/mm^2 specific energy, 0.64 mm layer thickness

Fig. 16 Sample E1. 200 J/mm^2 specific energy, 1.37 mm layer thickness

Fig. 17 Sample D2. 59 J/mm^2 specific energy, 0.25 mm layer thickness

the majority of the clad consists of columnar grains. The microstructure changed similarly within the power, velocity and powder mass flow rate design of experiments matrix.

The major factors in determining the microstructure are specific energy as well as layer thickness. These parameters are dependent on each other as described above. As the specific energy is lowered, the layer thickness is less because there is less energy per unit area to melt powder. For the highest specific energy used, which is 200 J/mm^2, the layer thickness varied between 0.64 mm to 1.37 mm (samples C16 and E1, respectively), depending on the powder feedrate used. The microstructure for the sample with the 0.64 mm layers, Sample C16, had much more defined regions of microstructure where the average primary dendrites were around 8 microns wide. A picture of this microstructure near the interface region is provided in Fig. 15. This sample had an interface layer about 50 microns thick and a columnar region which was about 120 microns thick, while the rest of the layer was composed of equiaxed grains. The part with the 1.37 mm layers, Sample E1, had a small interface region, 40 microns thick, a small columnar region, approximately 70 microns thick and the rest of the layer was composed of equiaxed grains. The columnar region is shown in Fig. 16. The average grain width was between 12 to 20 microns, which about 2 times larger that of the part with the 0.64 mm layer thickness. In another case, the layer thickness was held constant at 0.25 mm and the specific energy was changed from 59 J/mm^2 to 39 J/mm^2. The change in specific energy was due to the velocity being increased from 17 to 25 mm/s, corresponding to samples D2 and E11, respectively. In this case, the structure in E11 has primary dendrite widths of 2–4 microns, while sample D2 has primary dendrite widths of 4 to 10 microns. This microstructure is shown in Figs. 17 and 18. In the equiaxed regions for both samples it was difficult to get a clear measurement of the primary dendrite size, but the structure in E11 was appro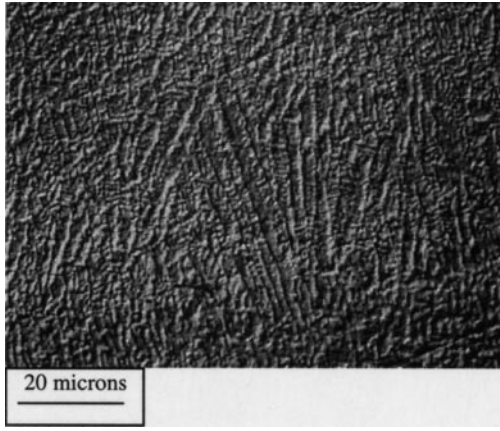ximately half the size of that in D2. In summary, the primary dendrite widths become larger with an increase in either layer thickness or specific energy. Several other parameter changes were made in order to see if they had a significant effect on

Fig. 18 Sample E11. 39 J/mm² specific energy, 0.25 mm layer thickness

microstructure. These are process gas flow rate and cladding pass overlap. Microstructure was found not to be affected by the changing of either the Helium shielding gas flow rate or the Nitrogen powder assist gas flow rate. In the case of changing the amount that each cladding pass overlapped, there were some small effects on microstructure.

Secondary dendrite arm spacing (SDAS)

Another microstructure characteristic that was affected by the layer thickness and specific energy was the secondary dendrite arm spacing, which is representative of the cooling rate of the deposited metal. In each cladding pass, the secondary dendrite spacing changed somewhat depending on which microstructure region it was located. In the interface region, the secondary dendrite arm spacing was found to be 5 to 10 times larger than that in the columnar and equiaxed dendrite regions. In some cases, secondary dendrites could not be found in the interface region. The columnar and equiaxed dendrite regions have similar secondary dendrite arm spacing, but some variation, sometimes up to 40%, was not unusual. According to Kurz and Fisher [28], secondary dendrite spacing can be used to estimate the cooling rate by the following equations:

$$\dot{T} = \frac{\Delta T}{t_f}$$

where t_f can be found from

$$\lambda_2 = 5.5(Mt_f)^{1/3}$$

with

$$M = \frac{\Gamma D ln(\frac{C_l^m}{C_o})}{m(1-k)(C_o - C_l^m)}$$

where C_l^m is often equal to C_e.

$\Delta T'$ dendrite tip to root temperature difference, and in this case is approximated by ΔT_0
ΔT_0 Liquidus-solidus temperature range at C_0 (K)
t_f Time of solidification (s)
λ_2 Secondary dendrite arm spacing (SDAS) (m)
Γ Gibbs-Thomson coefficient (Km)
D Diffusion coefficient in liquid (m²/s)
C_l^m maximum liquidus concentration value (wt%)
C_e eutectic composition (wt%)
C_0 initial alloy concentration (wt%)
m liquidus slope (K/wt%)
k distribution coefficient

Using typical property values for 0.35 wt% C steel, the above equations can be consolidated into a single equation as follows:

$$\dot{T} = \frac{1}{\lambda_2^3}(3.87 \times 10^{-13} \frac{Km^3}{s}).$$

λ_2 was determined by taking an average of the secondary dendrite arm spacing from a cladding pass in the center of the specimens. Using the previously defined equation, the cooling rates were found to be on the order of 10⁵ K/s. These cooling rates are extremely high in comparison to cooling rates obtained by traditional methods, but this is typical in laser material processing.

This cooling rate can be changed by two factors, which are layer thickness and specific energy. From Fig. 19, which is a plot of layer thickness vs. cooling rate for the measurements taken from samples in the power, velocity, and powder mass flow rate test matrix, it is obvious that the cooling rate increases as the layer thickness decreases. In one example, doubling the layer thickness from 0.3 mm decreased the cooling rate by one-half of the original. In Fig. 20, it is shown that the cooling rate can be increased as the specific energy is decreased. From the linear fit of points, it can be seen that as the adjusted specific energy is changed from 100 to 50 J/mm², the cooling increases by approximately 2.5 times its original to 2.5×10⁵ K/s. It may seem that the cooling rate is determined only by the specific energy since layer
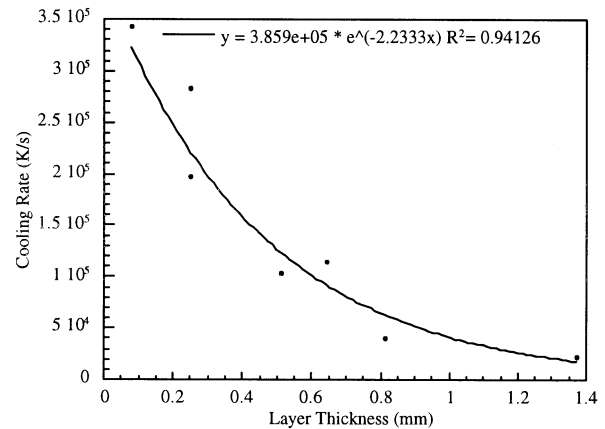
Fig. 19 Influence of layer thickness on cooling rate
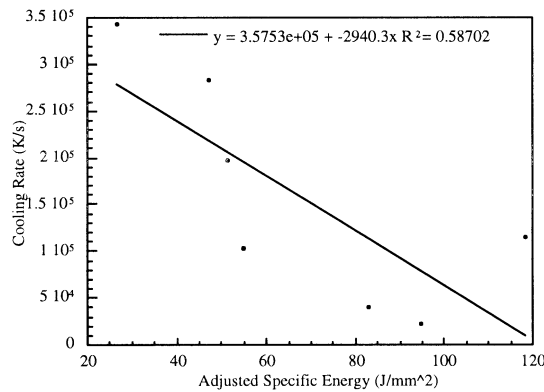
Fig. 20 Inverse relationship between specific energy and cooling rate

thickness increases as the specific energy increases, but this is not the case.

The cooling rate is determined by the combination of effects from both parameters. To show this, one example of each case will be given. In the first case, the layer thickness was held constant at 0.25 mm, while the specific energy was changed from 59 to 39 J/mm² (samples D2, E11 respectively). This decrease in specific energy resulted in a cooling rate increase of about 40% from the original. In the other case, specific energy was held at 39 J/mm² while the layer thickness was changed from 0.25 mm to 0.08 mm (samples E11 and C22, respectively), and the cooling rate increased by about 15%. It should be noted that the dendrite arm spacing values used for these comparisons are average values for a single cladding pass. Due to the variation in dendrite arm spacing within each clad, similar dendrite arm spacing, and hence cooling rates, have been found between the different cases. So from these two cases, it is shown that the average cooling rate was affected by the process specific energy as well as the layer thickness.

The cooling rate was also affected by percent overlap between cladding passes. As the overlap increased from 27 to 74 percent, the cooling rate increased by approximately 20%. This sounds like it contradicts what was said in the last section, because as the percent overlap increases the layer thickness increases. This increased layer thickness should have an inverse effect on the cooling rate. But if the deposition geometry of the cladding pass, is closely examined, it can be seen that even though the overall height is increased, the clad width decreases, making the cladding pass longer and more slender than a cladding pass with low overlap. Since the overall deposition geometry gets thinner as the percent overlap increases, the cooling rate also increases. This is consistent with the previous conclusions.

The gas flow rate study showed that there were no significant effects on cooling rate from changing the gas flow rates. Overall, the specific energy, cladding layer thickness, and pass overlap each effected the grains in each cladding pass, as well as the cooling rates.

Microhardness

There are many factors that affected the microhardness within the samples. These factors included location within the sample tested and changes in process parameters. Overall, the hardness was found to be between 450 and 580 Vickers hardness.

Influence of location

The microhardness within the three regions of a single cladding pass were tested in several samples that had different base parameters. The hardness was found to change, in most cases, for the equiaxed, columnar, and interface regions. No significant conclusions can be drawn about the hardness differences between the equiaxed and columnar regions since their hardness values were typically less than five percent different. This five percent variation did not favor either region. Note: All hardness values that were used for comparison purposes were taken from an average of at least three hardness measurements in the same region. The interface region, however, did have up to a ten percent lower value for microhardness in comparison to the equiaxed and columnar regions. This lower hardness is expected since the interface region is essentially re-melted or re-heated material. When the underlying cladding pass is re-melted, it is annealed or heat-treated, therefore losing some of its hardness. On a larger scale, the hardness also was found to vary over the whole sample.

In order to show the variation of hardness over a whole sample two arrays of measurements were taken. These measurements were all taken in the center of the cladding passes to keep the measurements more consistent with each other, and so other factors would not affect any trends.

One of the sets of measurements traversed the sample from the top surface down into the substrate. The results from this set of measurements, as plotted in Fig. 21, show
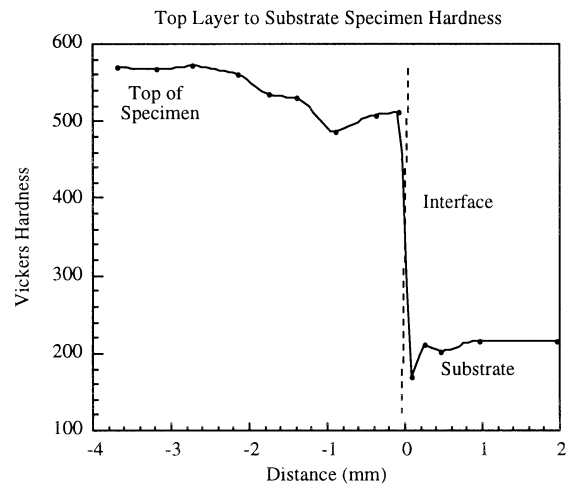
Fig. 21 Specimen hardness: top to bottom of sample
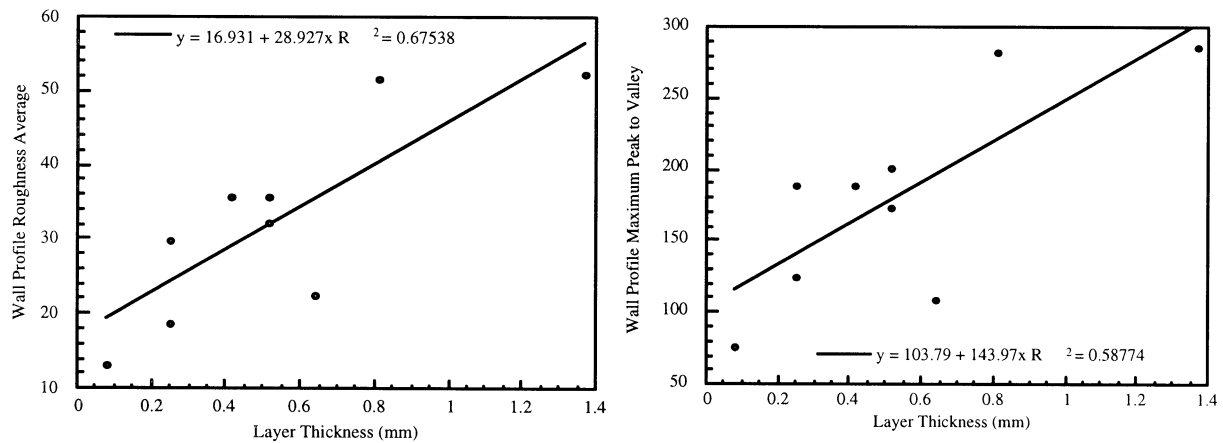
Fig. 22 Influence of layer thickness on wall roughness

that the material was hardest at the top surface and became softer towards the bottom of the sample. And of course the substrate material was much softer, since it was a mild steel. The bottom layers of the sample were softer than the top layers because they had a longer temperature history. In other words, as layers of cladding were added to the sample, the previous layers were heated up again, giving them time to slightly anneal each time.

Special cases

A couple of samples were made at higher speeds in order to push the current process operating envelope. The traverse speed in this case was 51 mm/s, which is twice as fast as what was used previously for the maximum speed. In this case the specific energy was much lower than any of the previous sets of process parameters. The layer thickness was set to 0.25 mm and percent pass overlap to 66 percent, and as a result the hardness was 54.4 Rockwell C or 584 Vickers. The sample that most closely matched the processing parameters of this special case had the same layer thickness, 27 percent pass overlap, and a specific energy of 31.5 J/mm^2, which is 1.7 times greater than that of the special case specimen (18.7 J/mm^2). From this comparison, it seems that the lower specific energy definitely has a strong effect on hardness.

Comparison with wrought H13 tool steel

The direct metal deposition manufactured H13 metal samples were shown to have similar hardnesses as wrought H13 tool steel. For wrought H13 tool steel, the typical working hardness is between 40 and 53 Rockwell C hardness and an as-quenched hardness of 50–54 R_c [29, 30]. This is very similar to the 46 to 54 Rockwell C hardness material that was fabricated during this study. Once larger parts are made with the H13 metal powder using the direct metal deposition process, some of the hardness may be lost due to heat treating by repeated heating of the material, which is inherent of the process. The resulting hardness by this process is comparable with wrought material, but the surface finish is not close to that of a machined material.

Surface roughness

Surface roughness was found to vary depending on which direction the measurements were taken with respect to the cladding. In checking the surface roughness, four directions were tested from each sample; the length and width directions on the top surface, and the horizontal and vertical directions on the walls. From a few initial measurements it was found that the roughness in the vertical direction on the side wall was approximately three percent greater than the horizontal direction. On the top surface, the roughness perpendicular to the cladding, which was the lengthwise direction in this case, was found to be about five percent rougher than parallel to the cladding. Since the largest roughness on each sample was of primary interest, measurements were only taken perpendicular the clad direction on the top surface and in the vertical direction on the walls.

Wall roughness

Within the power, velocity and powder mass flow rate study, the wall profile roughness averages were found to vary between 13 and 51 microns, while the wall maximum peak to valley distances ranged from 75 to 275 microns. These roughness were found to both be directly related to the layer thickness. As shown in Fig. 22, the wall roughness can significantly be reduced by making the deposition layers thinner. The reason why the wall surface gets rougher as the layer thickness increases is due to the beam diameter variation due to defocusing. As the layers become thicker, the beam diameter has a longer distance to diverge. Therefore, the width of cladding is larger at the bottom of the cladding pass in comparison to the top of the cladding pass. By reducing the layer thickness, this beam diameter variation is also reduced and therefore the specimen wall roughness is minimized.
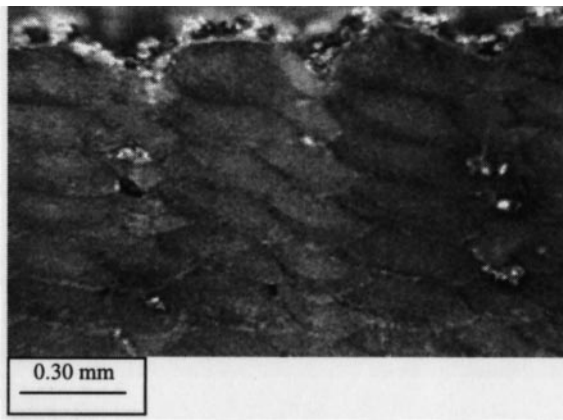
Fig. 23 Cross-sectional view of a specimen made with single sensor
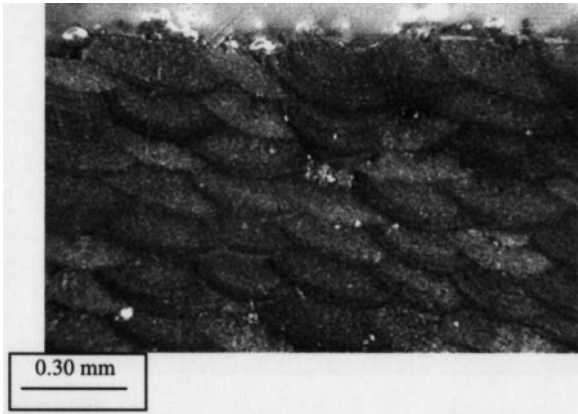
Fig. 24 Cross-sectional view of a specimen made with multiple sensors

In cases with higher deposition velocities, there was a problem with wall quality. With higher velocities, the cladding at the sample edges sometimes was not able to catch as much powder as the internal sample cladding. Eventually, the cladding was unable to build up fast enough to compensate for this condition, creating gaps in the cladding passes at the sample edges. By reducing the traverse speed of the deposition around the outline of the part, there is enough time for the clad to build to the required height eliminating any defects.

Effect of height controller on direct metal deposition

The height controller has a significant part in the direct metal deposition process since it has control over the laser power. This also has the potential of causing problems if it is not set up correctly. One of the important control parameters was found to be the controller reset time.

Influence of multiple sensors on laser power control

As described in the experimental set-up, three sensors were constructed along with a new controller in order
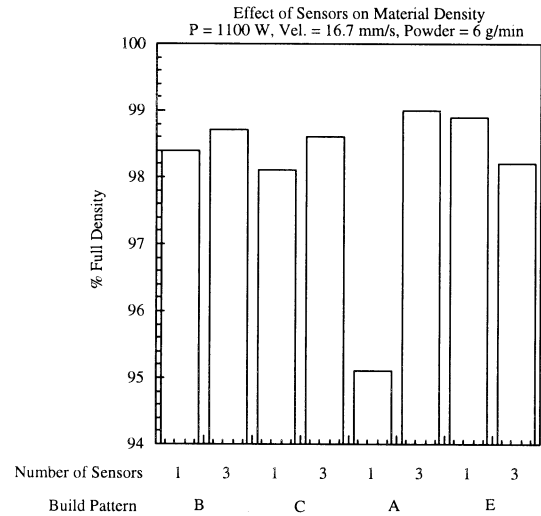

Fig. 25 Effect of sensors on material density

to improve the height control of the direct metal deposition process. The height control was to be improved by eliminating any laser power fluctuations during processing. A single height sensor's ability to sense the melt pool height is dependent upon the direction of cladding. As the cladding path is directed away from the sensor, the solidified clad bead hides most of the melt pool light from the sensor, resulting in a false reading that the melt pool is too low. In this case, the laser power will be allowed to go to the set maximum power (duty cycle of laser = 100%), building slightly higher than the set maximum height limit. When the cladding path is directed towards the sensor, the melt pool is easily seen, and the sensor behaves normally, shutting off the laser power only when the melt pool height gets to the maximum limit. In some cases, the duty cycle of the laser power is close to zero as the cladding is directed towards the sensor immediately after a laying down a clad bead traversing away from the sensor. This is because the previous pass built up too much material, and during the clad that takes place towards the sensor, this added height is detected, making the duty cycle drop to a very low value since the melt pool is too high.

Influence of multiple sensors on material properties

In order to show the benefit of multiple sensors, several primary build configurations were used: patterns B, C, and D. These build patterns are detailed in Fig. 6. The build pattern B is the weakest building pattern for the single sensor configuration, since it best shows the power fluctuations as described above.

For a cross-sectional view of the sample made with this build configuration (B) with a single height sensor, see Fig. 23. The high and low power fluctuations for the single sensor configuration will give large and small volume cladding passes as shown in this figure. And in Fig.
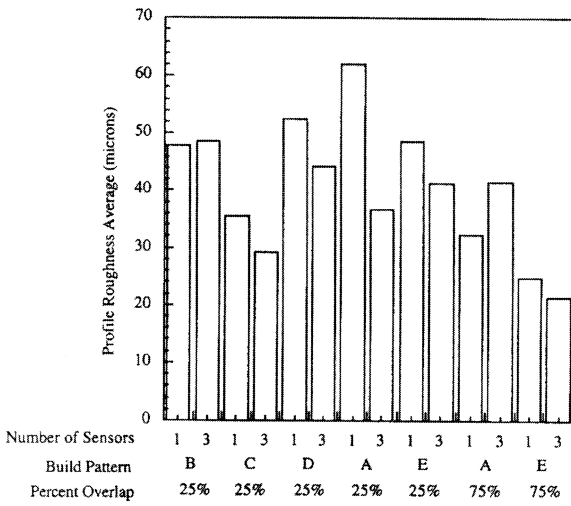
Fig. 26 Effect of sensors on roughness average (microns)
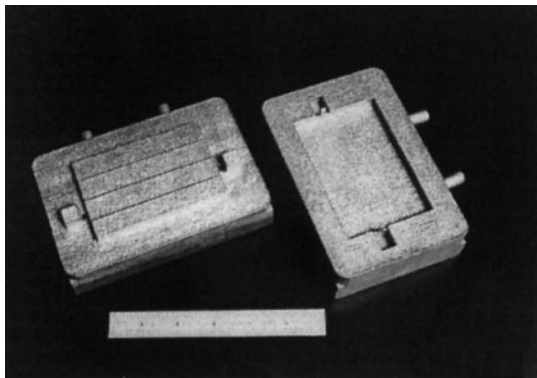
Fig. 27 Injection molding dies with imbedded copper chiller block and a water-cooling channel

24, it can be seen that the cladding passes are consistently the same size for a multiple sensor height controller. The microstructure in each case was examined closely and it was found that there was no variation between the samples made using either of the sensor configurations. Hardness was found to vary less than one percent be-

tween the two samples. Density, on the other hand, was found to vary slightly, as shown in Fig. 25.

This lower density in case three, +XY or build pattern A, is due to the fact that lower-powered material processing has a tendency to leave porosity behind, and in the case of a single sensor, there are many cladding passes with low laser power due to inconsistent material deposition rates.

Influence of multiple sensors on surface roughness

The three sensor system proved to be effective in reducing the surface roughness average of the fabricated parts by approximately 14 percent. In other words, from an average of 7 different specimen sets (5 different build patterns and 2 more with higher pass overlap), the three sensor configuration reduced the profile roughness average from 44 microns to 38 microns. And at the same time reduced the average maximum profile roughness height from 270 microns to 210 microns, or a 22 percent improvement. As was stated before, the maximum profile roughness height is the maximum surface peak to valley measurement. Figure 26 shows surface roughness measurements from parts made with one and three sensors.

Application

The Direct Metal Deposition (DMD) process has been successfully applied to fabricate injection molding dies with imbedded copper chill block and copper cooling channel (Fig. 27). This has the potential for improved thermal management and theoretical calculation shows that the cycle time can be reduced by 50%. Recently, ZrO_2 was co-deposited with nickel superalloys using DMD (Fig. 28), which is another example for improved thermal management. The group at the University of Michigan is now working to merge the DMD with Homogenization Model and CAD representation to fabricate designed microstructure. This process thus is ame-

Fig. 28 Co-deposition of ZrO_2 and Ni superalloy

Ceramic Top Coat, Y-PS2

Metallic bond coat, NiCrAlY
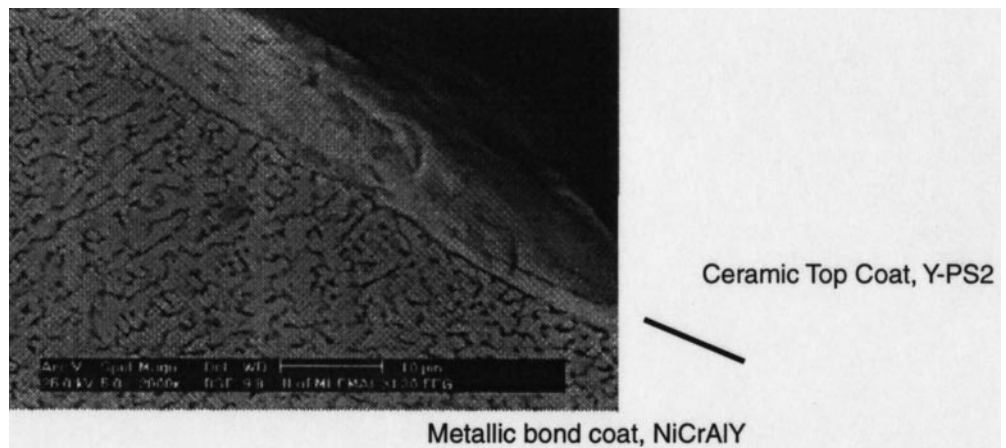
nable to produce both macro and microstructure to a designed specification.

Summary and conclusion

This paper presented the effect of independent parameters on the resulting characteristics of the fabricated parts and the process. The relationships between increasing layer thickness due to increasing specific energy and percent pass overlap were developed. It was also found that when the process energy/mass ratio dropped below 40 KJoules/gram, the density of the fabricated material was less than 96% full theoretical density.

In the usable range of direct metal deposition, it was found that deposition rates of up to 300 mm^3/s and powder utilization efficiencies up to 30% could be obtained. The typical processing values were around 100 mm^3/s and 15% for these parameters, respectively.

It was also found that microstructure stays consistent throughout a fabricated sample. By decreasing specific energy, decreasing layer thickness, increasing speed, both finer grains and higher cooling rates were obtained. The cooling rates observed in this process typically were on the order of 10^5 K/s.

Hardness was found to be similar to that of wrought material. Internal sample hardness slightly decreased towards the middle and bottom of part due to the re-heating of the material that occurs during processing.

Surface roughness was found to be on the order of 40 microns, and was reduced approximately 20% by increasing the percent overlap.

By understanding these relationships between parameters and their effect on the process output, the process can be used more effectively and the quality can be improved.

The density of parts was increased with the shortening of the reset time for the controller. Also, the number of sensors in the height controller was increased, eliminating the directional dependence of the height controller on material deposition. The addition of the two sensors had no major overall effect on material properties of the fabricated parts, but it did slightly increase the material density in one case. The most important improvement of the multiple sensor height controller is that the roughness of the surfaces can be reduced on average 14 to 20%.

From this study, the capabilities and of fine cladding with H13 tool steel have been quantified as well as the effects of the process parameters on the fabricated parts. The understanding and addition of height sensor capability has improved upon the previous process fabricated part quality.

References

1. Koch JL, Mazumder J (1993) In: Denney P, Miyamoto I, Mordike BL (eds) Rapid prototyping by laser cladding, ICALEO, vol 77. Orlando, FL, p 556
2. Chun JH, Passow CH (1993) Droplet based manufacturing. Conference in International Rapid Prototyping
3. Acquaviva PJ, Nowak T, Chun JH (1994) Issues in application of thermal spraying to metal mold fabrication. International Body Engineering Conference (IBEC '94)
4. Orme M (1991) The Physics of Fluids A 3:2936
5. Orme M (1993) The Physic of Fluids A 5:80
6. Orme M (1993) Rapid solidification materials synthesis with nano-liter droplet. Education, Training, and Human Engineering in Aerospace: Aerotech '93, SAE International, Costa Mesa, CA
7. Westmoreland J (1995) National Center for Manufacturing Science, private communication
8. Bunnell DE, Bourell DL, Marcus HL (1996) Solid freeform fabrication of powders using laser processing. In: Advances in powder metallurgy and particulate materials, part 15. MPIF, p 93
9. House MA, Whitney EJ, Krantz DG, Arcella FG (1996) Solid Freeform Fabrication Symposium, University of Texas at Austin, p 239
10. Merz R, Prinz FB, Ramaswami K, Terk M, Weiss LE (1994) Solid Freeform Fabrication Symposium, University of Texas at Austin, p 1
11. Fessler JR, Merz R, Nickel AH, Prinz FB, Weiss LE (1996) Solid Freeform Fabrication Symposium, University of Texas at Austin, p 117
12. Dickens PM, Pridham MS, Cobb RC, Gibson I, Dixon G (1992) Solid Freeform Fabrication Symposium, University of Texas at Austin, p 280
13. Dave VR, Matz JE, Eager TW (1995) Solid Freeform Fabrication Symposium, University of Texas at Austin, p 64
14. Ribeiro AF, Norrish J (1996) Solid Freeform Fabrication Symposium, University of Texas at Austin, p 249
15. Orme M, Huang C, Courter J (1995) TMS Annual Meeting, p 125
16. Griffith ML, Keicher DM, Atwood CL, Romero JA, Smugeresky JE, Harwell LD, Green DL (1996) Solid Freeform Fabrication Symposium, University of Texas at Austin, p 125
17. Keicher DM, Romero JA, Atwood CL, Smugeresky JE, Griffith ML, Jeantette FP, Harwell LD, Green DL (1996) Advances in Powder Metallurgy and Particulate Materials, part 15. MPIF, p 119
18. Schanwald LP (1996) Advances in Powder Metallurgy and Particulate Materials, part 15. MPIF, p 139
19. Mah R (1997) Advanced Materials and Processes 151:31
20. Lewis GK, Thomas DJ, Nemec RB, Milewski JO (1996) Advances in Powder Metallurgy and Particulate Materials, part 15. MPIF, p 65
21. Mazumder J, Koch J, Nagarathnam K, Choi J (1996) Advances in Powder Metallurgy and Particulate Materials, part 15. MPIF, p 107
22. Mazumder J, Choi J, Nagarathnam K, Koch J, Hetzner D (1997) JOM 49:55
23. Breinan EM, Kear BH (1978) Rapid solidification laser processing of materials for control of microstructure and properties. In: Proc of Conf on Rapid Solidification Processing at Reston, VA. Claitor's Publishing Div, Baton Rouge, LA, p 87
24. US Patent No 4724255, Quantum Laser Corporation, Atlanta, GA
25. Mazumder J, Voelkel DD, US Patent No 5,446,549
26. Koch JL, Mazumder J (1995) Patent Disclosure No 95038, University of Illinois
27. Tewari S, Mazumder J (1993) Patent Disclosure No T93043, University of Illinois
28. Kurz W, Fisher DJ (1986) Fundamentals of solidification. Trans Tech Publishing, Rockport, MA
29. Roberts GA, Cary RA, Tools Steels, 4th ed. American Society for Metals, Metals Park, OH pp 64, 276, 578
30. Davis JR et al (eds) (1990) Metals Handbook: Properties and Selection: Irons, Steels, and High-Performance Alloys, 10th ed, vol 1. ASM International, Materials Park, OH, p 757